Carbohydrate Polymers 82 (2010) 329–336

Contents lists available at ScienceDirect

Carbohydrate Polymers

journal homepage: www.elsevier.com/locate/carbpol

Preparation and properties of cellulose nanocrystals: Rods, spheres, and network

Ping Lu, You-Lo Hsieh*

Fiber and Polymer Science, University of California, One Shields Avenue, Davis, CA 95616, USA

ARTICLE INFO

Article history:
Received 6 March 2010
Received in revised form 21 April 2010
Accepted 22 April 2010

Keywords:
Cellulose nanocrystals
Acid hydrolysis
Freeze-drying
Mesoporous structure

ABSTRACT

Cellulose nanocrystals with rod, sphere, and network morphologies were prepared by acid hydrolysis of cotton cellulose, followed by freeze-drying. Hydrolysis with sulfuric acid introduced sulfate groups to these nanocrystal surfaces permitting their dispersion in aqueous as well as organic media, including ethanol and N,N-dimethylformamide, in a matter of seconds. Freeze-drying, on the other hand, induced mesoporosity (91.99 ± 2.57 Å average pore width) and significantly improved specific surface ($13.362\ m^2/g$) that is about 9 times of the original cellulose ($1.547\ m^2/g$). Moreover, the nanocrystals exhibited improved thermal conductivity and considerably higher (nearly 30%) carbonaceous residue, possibly due to direct solid-to-gas decomposition. These results demonstrated that a combination of surface charge introduction and fixation of mesoporosity in cellulose nanocrystals is an efficient route to prepare large quantity of high quality cellulose nanocrystals with quick re-dispersion capability for practical applications.

1. Introduction

Cellulose, the most abundant biomass in the world, is a linear syndiotactic homopolymer of β-(1 → 4)-glycosidic bonds linked D-anhydroglucopyranose (Kim, Yun, & Ounaies, 2006). Native cellulose is generally known to be fibrillar and crystalline (Saxena & Brown, 2005) and the cellulose fibrils play a significant role in contributing to the high strength of plant cell walls (Zuluaga et al., 2009). Crystalline nanofibers with crystallinities from 65% to 95% have been extracted from a broad range of natural sources including cotton (Favier, Chanzy, & Cavaille, 1995), tunicate (Terech, Chazeau, & Cavaille, 1999), algae (Hanley, Giasson, Revol, & Gray, 1992), bacteria (Grunert & Winter, 2002) and wood (Beck-Candanedo, Roman, & Gray, 2005). These cellulose fibrils were reported to be 2–20 nm wide. Their aspect ratios varied from 40 (~200 nm long and 5 nm wide) for cotton to around 66 (~1 μm long and 15 nm wide) for tunicin whiskers (Samir, Alloin, & Dufresne, 2005).

The bending strength and modulus of the cellulose nanofibrils estimated (Helbert, Cavaille, & Dufresne, 1996; Sakurada, Nukushina, & Ito, 1962; Sturcova, Davies, & Eichhorn, 2005) and measured by Raman spectroscopy (Sturcova et al., 2005) were impressively high at ~10 and ~150 GPa, respectively. Cellulose nanofibers thus have a bending strength that is nearly one-sixth of the 63 GPa for the carbon nanotubes whose tensile strength is predicted to be as high as ~300 GPa at E of ~1 TPa (Wong, Sheehan, & Lieber, 1997; Yu et al., 2000), but can be prepared far more economically from readily available renewable resources. Various cellulose nanofibrils, nanocrystals and whiskers have been incorporated into polymer matrices to produce reinforced composites with several tens to hundreds folds higher mechanical strength (Beecher, 2007; Lu & Hsieh, 2009; Svagan, Samir, & Berglund, 2008) as well as enhanced optical transparency (Ifuku et al., 2007). Cellulose nanofibrils have been used as substrates to determine cellulase activity (Helbert, Chanzy, Husum, Schuelein, & Ernst, 2003) and as carriers for targeted delivery of therapeutics (Dong & Roman, 2007). With the layer-by-layer (LbL) technique, cellulose nanowires have been assembled into antireflective films (Podsiadlo et al., 2007) and high performance nanocomposites (Podsiadlo et al., 2005).

The major challenge of developing the cellulose nanofibers as advanced materials and for further applications is their tendency to form bundles or aggregates. During drying, the abundant hydrogen bonds of cellulose draw the cellulose nanocrystals together to pose significant problems in their re-dispersion for effective processing (Tingaut, Zimmermann, & Lopez-Suevos, 2010). To enable better utilization, it is crucial to develop methods to isolate the nanofibrils after the solvent evaporation in their preparation.

This study was to investigate the hydrolysis and drying processes with the intent to minimize hydrogen bonding, thus reduce and even eliminate aggregation of the cellulose nanocrystals. Homogenous and stable cellulose nanocrystals suspensions were generated by hydrolyzing native cellulose with sulfuric acid to introduce negative charges to the nanocrystal surfaces. Esterifi-

* Corresponding author. Tel.: +1 530 752 0843; fax: +1 530 752 7584.
E-mail address: ylhsieh@ucdavis.edu (Y.-L. Hsieh).

0144-8617/$ – see front matter © 2010 Elsevier Ltd. All rights reserved.
doi:10.1016/j.carbpol.2010.04.073

cation of surface hydroxyl groups of cellulose nanocrystals has shown to introduce sulfate groups to form stable suspensions (Beck-Candanedo et al., 2005). The focus was then to prevent hydrogen bond formation by sustaining repulsion among the cellulose nanocrystals with fast freezing of water among the well-dispersed cellulose nanocrystals with liquid nitrogen to keep them separated and fixed in the solidified ice. The high vacuum in freeze-drying then sublimates the ice in-between the cellulose nanocrystals to substantially reduce or prevent hydrogen bonding, the driving force for the cellulose nanocrystals to aggregate. The induced morphologies and properties of the cellulose nanocrystals were studied to relate to the hydrolysis and drying processes.

2. Experimental

2.1. Materials

Cotton cellulose from filter paper (Q2, Whatman) was purchased from Fisher Scientific (Pittsburgh, PA). Sulfuric acid (95–98%) for hydrolysis was provided by EMD (Gibbstown, NJ). Water used in all experiments was purified by a Millipore Milli-Q Plus (Billerica, MA) water purification system.

2.2. Sulfuric acid hydrolysis

The cellulose filter was milled (Thomas-Wiley Laboratory Mill model 4, Thomas Scientific, USA) to pass through a 60-mesh screen. Hydrolysis was performed using 64–65% (w/w) sulfuric acid (10 mL/g cellulose) at 45 °C for 60 min and stopped by diluting with 10-fold cold (4 °C) water (Beck-Candanedo et al., 2005). The suspension was washed once by centrifugation at 4500 rpm for 10 min and then was dialyzed using Fisherbrand (Pittsburgh, PA) regenerated cellulose dialysis membranes with 12–14 kDa molecular weight cut off and against ultra-pure water (Millipore Milli-Q UF Plus) until neutral pH was reached. The solid aggregates in the suspension were disrupted by sonication (Branson ultrasonic processor model 2510, Danbury, CT) for 2 h in an ice bath. The suspension was kept over ion-exchange resin (Rexyn I-300 H–OH from Fisher Scientific, Inc.) for 7 days and then filtered through Whatman 541 filter paper (Maidstone, Kent, England). The final concentration of the suspension was about 0.75% (w/w).

2.3. Freeze-drying

The cellulose nanocrystals suspension was quickly frozen by liquid nitrogen (N_2) in an ice-tray and the formed ice cubes were put into a freeze-dryer (FreeZone 1.0 L Benchtop Freeze Dry System, Labconco, Kansas City, MO) overnight to remove the solvent water. The ice cubes kept their shape during the entire freeze-drying process without any observable shrinkage. The dried product was stored in vacuum for the following characterizations.

2.4. Characterization

The concentration of produced cellulose nanocrystals in the suspension was determined by drying 5 mL suspension in air and the mass after water evaporation was weighed. Optical light microscope observations were performed by using a Leica DM2500. The magnifications used were 100× and 400× under crossed-polars. The microstructures and the surface morphologies of samples were examined by a scanning electron microscope (SEM) (XL 30-SFEG, FEI/Philips, Hillsboro, OR, USA) after gold coating (Bio-Rad SEM coating system). For transmission electron microscopy (TEM), the freeze-dried cellulose nanocrystals were re-dispersed into ethanol. A drop of 10 μl about 0.005% (w/v) cellulose nanocrystals suspension was added onto the carbon-coated electron microscopy grid (Ted Pella Inc., Redding, CA) and the excess liquid was absorbed by a filter paper. The specimens were then negatively stained with 2% uranyl acetate. Excess solution was blotted out with a filter paper and allowed to dry by evaporation at ambient condition. The sample grids were observed at 100 kV using a Philip transmission electron microscope (Philip CM 12). The fiber diameters and their distribution were evaluated by an image analyzer (analySIS FIVE, Soft Imaging System GmbH, Munster, Germany). The FTIR spectra were measured from 4000 to 400 cm^{-1} at a resolution of 4 cm^{-1} by a Nicolet 6700 spectrometer (Thermo Fisher Scientific, Pittsburgh, PA, USA). The thermal behavior of cellulose powder and nanocrystals was studied by differential scanning calorimetry (DSC) (DSC-60, Shimadzu, Japan) and thermogravimetric analyzer (TGA-50, Shimadzu, Japan) in N_2 at a heating rate of 10 °C/min from 30 to 500 °C (or 600 °C for TGA). The crystalline phases present in the samples were measured by X-ray diffraction (XRD) collected on a Scintag XDS 2000 powder diffractometer (Cupertino, CA) at 45 kV and 40 mA from 5° to 40° with a Ni-filtered Cu $K\alpha_1$ radiation (λ = 1.542 Å). The components of cellulose powder and cellulose nanocrystals were measured by the energy-dispersive X-ray spectroscopy (EDS). The surface areas, pore sizes and pore size distribution were measured by N_2 adsorption–desorption at 77 K or the Brunauer–Emmett–Teller (BET) method using a surface area and porosity analyzer (ASAP 2020, Micromeritics, Norcross, GA, USA).

3. Results and discussion

3.1. Preparation of cellulose nanocrystals and homogenous suspension

Acid hydrolysis of cellulose in sulfuric acid involves rapid protonation of glucosidic oxygen (path 1) or cyclic oxygen (path 2) by protons from the acid, followed by a slow splitting of glucosidic bonds induced by the addition of water (Fig. 1a). This hydrolysis process yields two fragments with shorter chains while preserving the basic backbone structure. In native cellulose, the amorphous regions are more accessible to acid molecules and susceptible to the hydrolytic actions than the crystalline region (Hon & Shiraishi, 1991). With sulfuric acid, the amorphous regions are digested very fast. Under the conditions employed, i.e., 60 min at 45 °C, most of the amorphous regions were removed leaving cellulose nanocrystals in the reaction solution.

Besides chain scission, hydrolyzing cellulose with sulfuric acid also involves esterification of the hydroxyl groups (Fig. 1b). This esterification reaction generally proceeds to yield acid half-ester or the so-called 'cellulose sulfate'. The presence of sulfate groups on the cellulose nanocrystal surfaces results in negatively charged surfaces above acidic pH. This anionic stabilization *via* the repulsion forces of electrical double layers was shown to be very efficient in preventing the aggregation of cellulose nanocrystals driven by hydrogen bonding (Marchessault, Morehead, & Koch, 1961). Observations during dialysis also confirmed this. The colloidal gel was observed at the beginning of dialysis when the cellulose nanocrystals suspension was still acidic, then disappeared as the pH became neutral with the removal of the residual acid. In order to avoid the possible desulfation of the sulfate groups on the surface of the cellulose nanocrystals, ultrasonic treatment was carried out in an ice bath.

3.2. Cellulose nanocrystals prepared by freeze-drying

Under crossed-polars of the optical microscope, the cellulose nanocrystals prepared by freeze-drying showed brighter color and more intensive contrast than the original cellulose powder, a clear

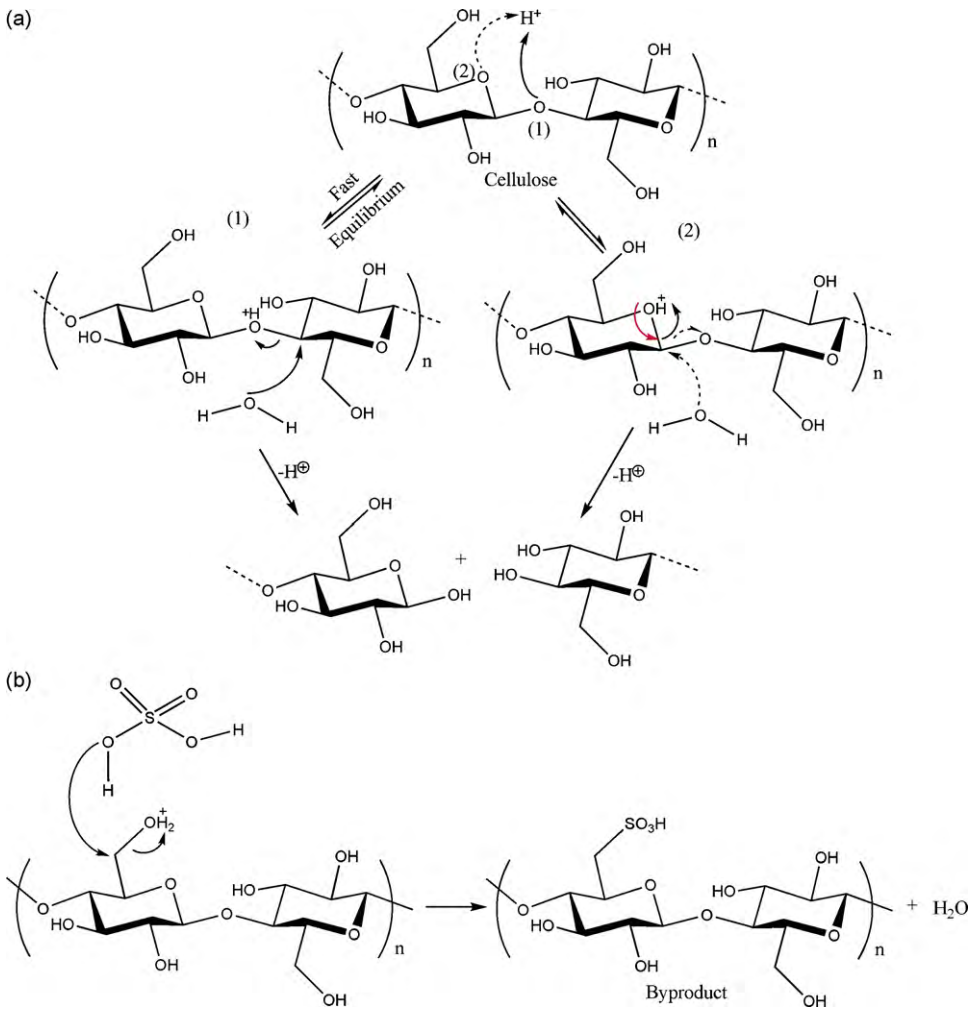

Fig. 1. (a) Acid hydrolysis mechanism and (b) esterification of cellulose nanocrystals surfaces.

indication of higher anisotropy (Fig. 2). This is expected from preferential acid hydrolysis of the less ordered regions in the cellulose, leaving the more highly crystalline cellulose aligned along the fibril's axis.

The SEM images of cellulose powder before acid hydrolysis clearly show the cellulose microfibrils (Fig. 3a and b). Following acid hydrolysis at 45 °C, these microfibrils in the original cellulose were swollen and separated into much smaller crystalline cellulose products in three forms, i.e., rods (Fig. 3c and d), spheres (Fig. 3e and f) and porous network (Fig. 3g and h). The most abundant form was the spherical nanocrystals while the least was porous network. These three different forms of nanocrystals could not be separated by the common methods of filtration and centrifugation. The TEM image of cellulose nanocrystal rods showed widths less than 10 nm and lengths between 200 and 400 nm (Fig. 3d). The rodlike cellulose nanocrystals appeared longer under the SEM, with lengths up to several microns and width in the range of 30–50 nm. It seems that some aggregations of cellulose nanocrystal rods did occur to

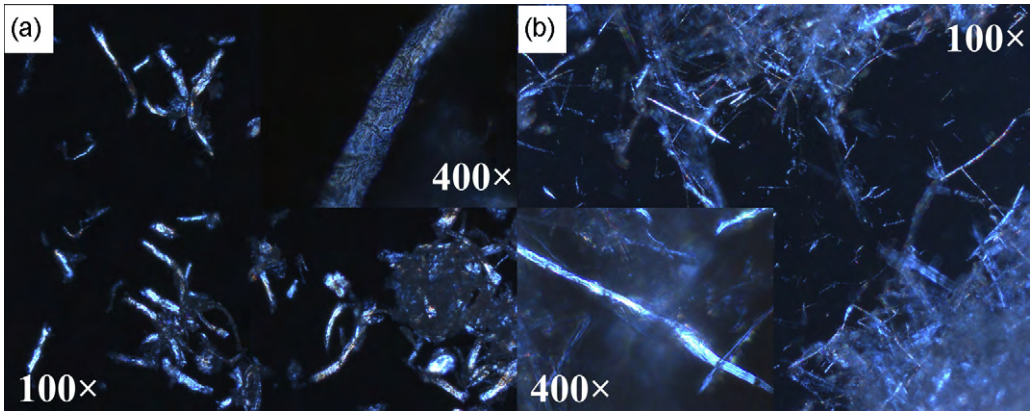

Fig. 2. Optical microscope images of (a) cellulose powder and (b) cellulose nanocrystals under crossed-polars.

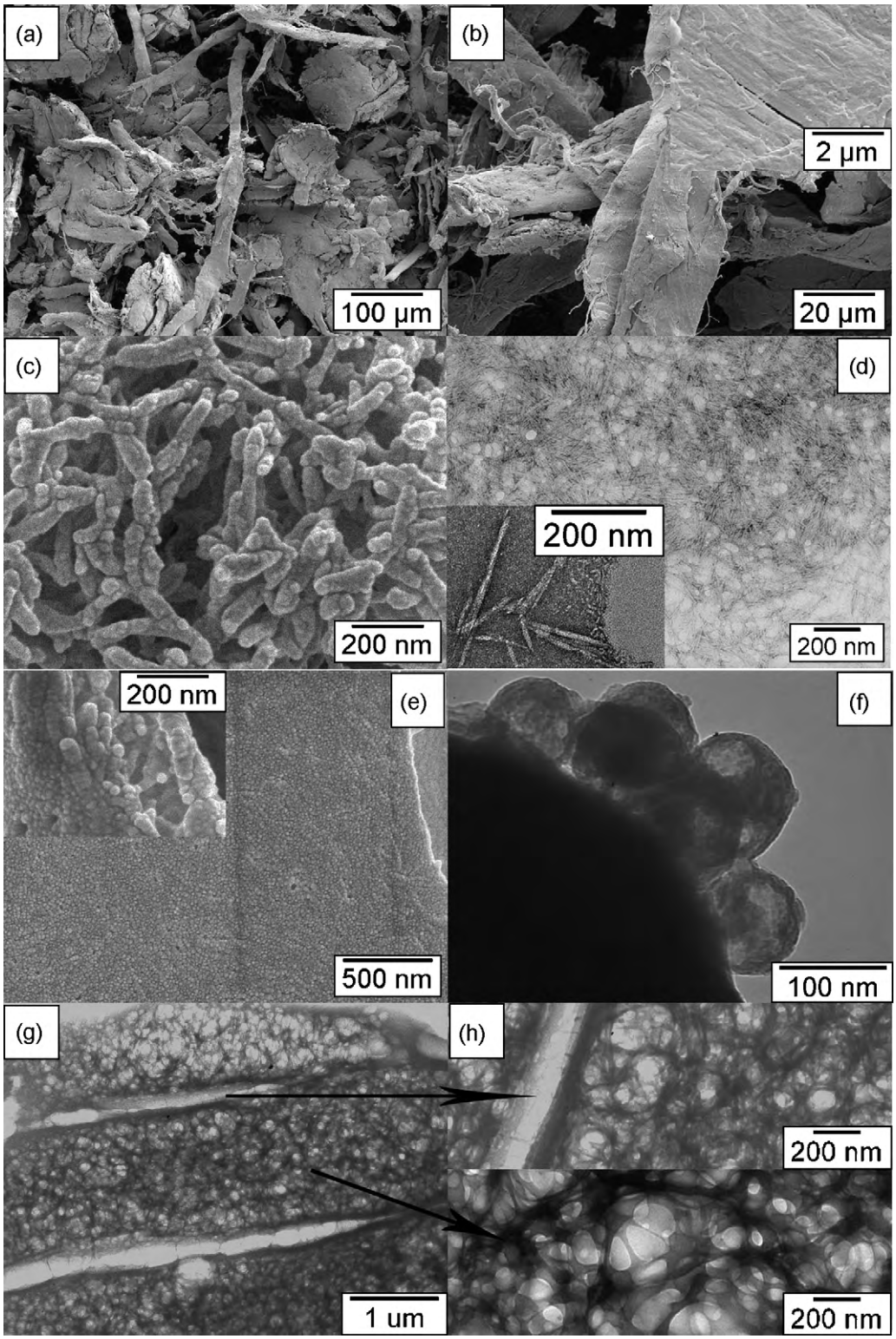

Fig. 3. SEM images of cellulose (a and b) powder and SEM (left, except g which is TEM) and TEM (right) images of nanocrystals in the forms of (c and d) rods, (e and f) spheres, (g and h) porous network.

form larger bundles during freeze-drying. However, these bundles of cellulose nanocrystals rods were loosely packed and easily separated by ethanol in preparing the TEM sample for observation. The majority of the products from acid hydrolysis and freeze-drying were spherical cellulose nanocrystals. The sources of these cellulose spheres (Fig. 3e) could be from self-assembled short cellulose rods *via* interfacial hydrogen bonds and/or the process involved in preparing cotton fibers into the filter paper. The spherical cellulose nanocrystals were loosely packed as shown by SEM (Fig. 3e) while the isolated spherical cellulose nanocrystals in 10–100 nm diameters were observed by TEM (Fig. 3f).

While rodlike and spherical cellulose nanocrystals by acid hydrolysis have been reported previously (Beck-Candanedo et al., 2005; Zhang, Elder, Pu, & Ragauskas, 2007), some network-

structured cellulose nanocrystals were also observed by TEM (Fig. 3g and h). The extended network in several microns in both the length and width directions was thought to result from the less dispersed cellulose nanocrystals in ethanol than in aqueous media. The strong H-bonding among cellulose nanocrystals overcomes the repulsion of surface negative charges, leading to the formation of self-assembled porous networks (van den Berg, Capadona, & Weder, 2007). These network-structured cellulose nanocrystals were not observed under SEM. It is possible that the network-structured cellulose nanocrystals were imbedded in the abundant spherical cellulose nanocrystals membranes in the freeze-drying process. Another possibility is that the network-structured cellulose was actually formed by the over-irradiation of electron beams during TEM observation. However, these network structures were even clearly seen in large quantities under low energy electron beam (80 kV). Therefore, further inquiry is needed to fully understand the source and formation of these cellulose networks observed by TEM. Most significantly, the cellulose nanocrystals prepared by freeze-drying could be directly dispersed into water, ethanol, DMF and other solvents in a matter of seconds without sonication. No aggregate except the networked cellulose was observed by TEM, indicating that the fibrils in the as-prepared cellulose nanocrystals samples were isolated. This easily dispersive behavior without aggregation in a wide range of common solvents is highly desirable for versatile processing and making many potential applications possible.

3.3. Chemical and crystalline structures of as-prepared cellulose nanocrystals

The original cellulose powders and nanocrystals showed similar FTIR spectra (Fig. 4A). The broad bands in the 3650–3000 cm^{-1} region are O–H stretching vibrations and the peaks at 2900 cm^{-1} correspond to C–H stretching vibrations. The 1430 cm^{-1} band can be assigned to bending of the –C-6 CH_2- while the deformation, wagging and twisting modes of the anhydroglucopyranose unit are observed from 1800 to 600 cm^{-1} and are consistent with others' reports (Mo, Zhao, Chen, Niu, & Shi, 2009). Both the cellulose powder and nanocrystals are cellulose Iβ type. Due to the different hydrogen-bonding strength of native cellulose Iα and Iβ, their O–H stretching and out-of-plane bending bands are different, i.e., stretching at 3240 cm^{-1} for Iα and 3270 cm^{-1} for Iβ and out-of-plane bending at 750 cm^{-1} for Iα and 710 cm^{-1} for Iβ (Wada, Kondo, & Okano, 2003). The crystalline Iβ characteristic peaks are present in the original powder as well as the nanocrystals: OH stretching at 3270 cm^{-1} and OH out-of-plane bending at 710 cm^{-1}.

The main differences in the FTIR are the stronger peak of the adsorbed water (H_2O) in the cellulose powders at 1641 cm^{-1} and the 1205 cm^{-1} sulfate peak of the cellulose nanocrystals from the esterification reaction. The presence of the sulfate groups was also confirmed by the EDS (Fig. 4B) where the cellulose nanocrystals had a weak sulfur peak which accounted for only 0.85 at% as compared to 64.38 at% for the carbon peak. This atomic ratio indicates that about 1 out 12 of the anhydroglucopyranose units reacted with sulfuric acid to form esters. This is consistent with the notion that the resultant sulfate groups were present mainly on the crystal surfaces and greatly improved the separation of nanocrystals by charge repulsion.

Both X-ray diffraction diagrams of cellulose powder (Fig. 5a) and nanocrystals (Fig. 5b) showed three cellulose I characteristic peaks at $2\theta = 14.7^\circ$, 16.4°, and 22.6° (Wada, Heux, & Sugiyama, 2004). The 22.6° peak of the (2 0 0) plane of cellulose nanocrystals becomes sharper, indicating higher perfection of the crystal lattice in the (2 0 0) plane than original cellulose. The peak for the $(1\,\bar{1}\,0)$ plane ($2\theta = 14.7^\circ$) also became more intense and separated from the 110 ($2\theta = 16.4^\circ$) peak for cellulose nanocrystals. The XRD results

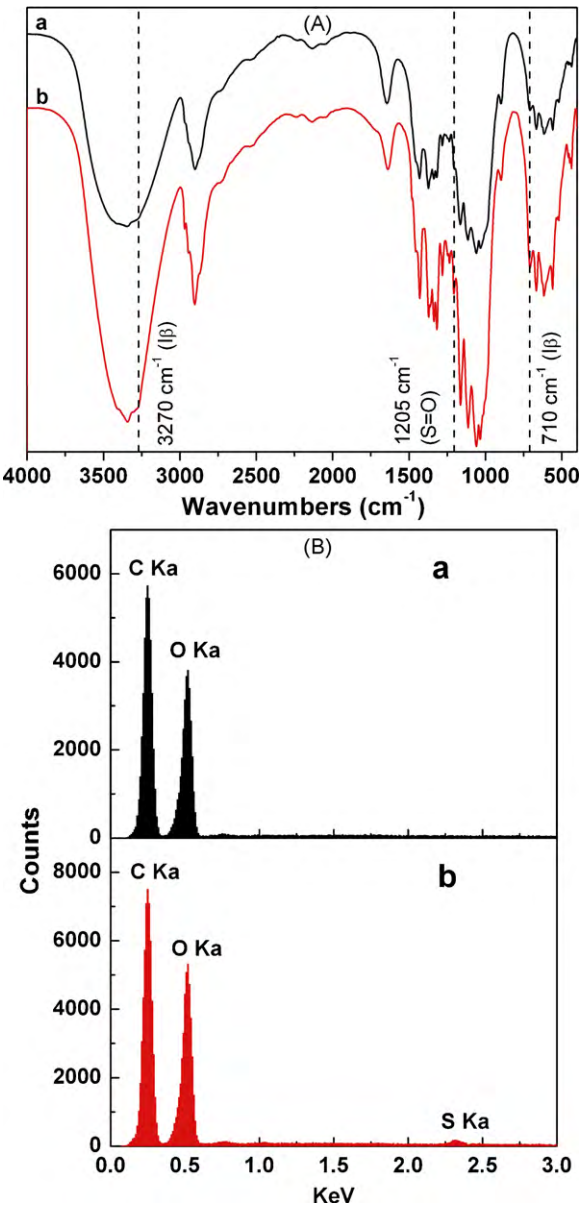

Fig. 4. (A) FTIR spectra of cellulose (a) powder and (b) nanocrystals. (B) EDS of cellulose (a) powder and (b) nanocrystals.

together with the FTIR data confirm that the cellulose nanocrystals retained the cellulose Iβ crystalline structure following the acid hydrolysis and freeze-drying process while becoming more crystalline than the original cellulose.

3.4. Thermal properties of cellulose nanocrystals

The cellulose nanocrystals also exhibited significantly different thermal behaviors than the original cellulose powders (Fig. 6). The original cellulose showed the typical decomposition with onset temperature just above 300 °C (Fig. 6A) and this coincided with a massive mass loss leaving only 2.87% ash at 600 °C (Fig. 6B). The cellulose nanocrystals, on the other hand, showed more gradual thermal transitions that started at a lower temperature around 150 °C in both DSC and TGA. The cellulose nanocrystals lost nearly 40% of its mass in the 150–300 °C region followed by another 30% mass loss between 300 and 600 °C, leaving significantly higher residue, nearly 30%, at 600 °C. These major thermal behavioral differences between the cellulose nanocrystals and the original cel-

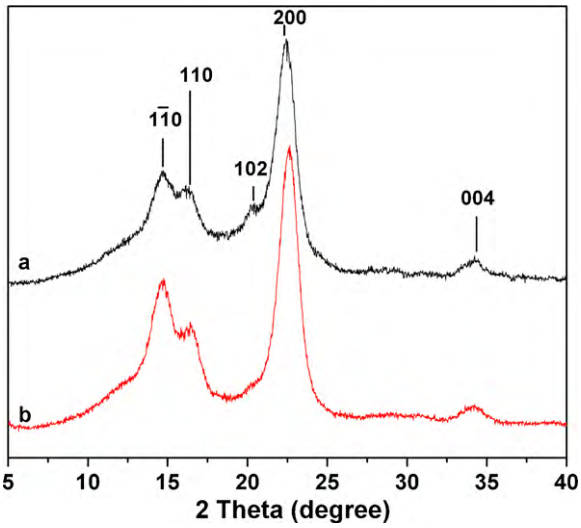

Fig. 5. XRD of (a) cellulose powder and (b) cellulose nanocrystals.

lulose powders may involve different decomposition–gasification processes. Cellulose is known to decompose to levoglucosan (1,6-anhydro-β-d-glucopyranose) at around 180 °C which then gasifies efficiently at 300 °C. This gradual mass loss of the cellulose nanocrystals in the 150–300 °C temperature range and the appearance of small endotherms around 160 and 210 °C suggest a different decomposition mechanism, possibly direct solid-to-gas phase transitions catalyzed by surface sulfate groups. It has been reported that the activation energies of the degradation of cellulose nanocrystals were significantly lowered by introducing sulfate groups *via* sulfuric acid hydrolysis (Roman & Winter, 2004). Therefore, the thermostability of cellulose nanocrystals was compromised by sulfate groups, agreed well with the above DSC and TGA results. Furthermore, the high surface area of cellulose nanocrystals might also play an important role in diminishing their thermostability due to the increased exposure surface area to heat. Moreover, the decomposition of cellulose nanocrystals occurring at lower temperatures from 150 to 300 °C might also indicate faster heat transfer in cellulose nanocrystals. The cellulose nanocrystals have been reported to function as efficient pathways for phonons, leading to their higher thermal conductivity (Shimazaki et al., 2007). The better thermal conductivity of cellulose nanocrystals might be ascribed to smaller phonon scattering in the bundle of crystallized cellulose chains in the cellulose nanocrystals than the amorphous random chains in cellulose powder. The lower weight loss of 70.25% (w/w) for cellulose nanocrystals indicated nearly one-third mass remained as the residue which was confirmed to be carbon by FTIR. This is also consistent with the proposed solid-state decomposition of cellulose nanocrystals. Since oxygen cannot be entirely eliminated in the circulating nitrogen in the DSC and TGA measurements, further improvement in the yield of amorphous carbon is highly possible.

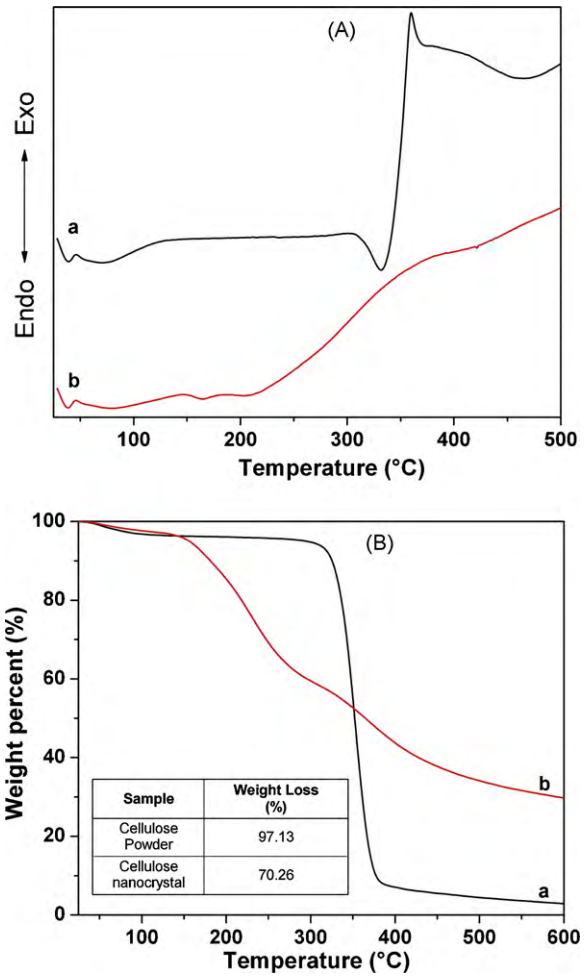

Fig. 6. DSC (A) and TGA (B) of cellulose (a) powder and (b) nanocrystals.

3.5. *Specific surface areas and pore structures of the freeze-dried cellulose nanocrystals*

The N_2 adsorption–desorption isotherms at 77 K of both the original cellulose (Fig. 7a) and the cellulose nanocrystals (Fig. 7c) are type IV accompanied by type H3 hysteresis, consistent with the report on cellulose (Sing et al., 1985). The Barrett–Joyner–Halenda (BJH) pore size distributions show that most pore diameters of freeze-dried cellulose nanocrystals are below 200 Å (Fig. 7d) while those of cellulose powders are above 200 Å (Fig. 7b), showing mesoporous structure in the cellulose nanocrystals. The mesopores which had a measured mean pore width of 91.99 ± 2.57 Å, are much smaller than the amorphous pores in the original cellulose with a mean pore width of 214.64 ± 7.23 Å (Table 1). Such mesopores could be present in the spheres and network structures, but not in the rods as confirmed by the SEM and TEM observations (Fig. 3). It is very possible that the mesopores also existed as the inter-crystal voids resulting from the evaporation of water and the corresponding driving force to move isolated cellulose nanocrystals closer.

The cumulative pore volume for cellulose nanocrystals ($0.03396 \pm 0.00059\ cm^3/g$) is 4 times larger than that for the original cellulose ($0.00839 \pm 0.00026\ cm^3/g$). The smaller cumulative pore volume of the original cellulose was expected with the rigid and highly hydrogen bonded cellulose structures. The pore volume of cellulose nanocrystals increased after loosely packed structures took shape to create a huge amount of mesopores among the nanocrystals. These mesopores can be clearly observed in the SEM images of the freeze-dried nanocrystals samples (Fig. 3). The same trend was observed with cumulative surface area of pores for cellulose powder and cellulose nanocrystals, but with much larger differences. The cumulative pores surface area of the cellulose nanocrystals ($14.771 \pm 0.158\ m^2/g$) was 10 times of that of the original cellulose powder ($1.563 \pm 0.019\ m^2/g$). While the original cellulose possessed $0.0910\ m^2/g$ micropores in its structure, the negative *Y*-intercept calculated in *t*-plot (not shown here) for cellulose nanocrystals indicated absence of micropores. This result suggests that aggregation by strong hydrogen-bonding effect in air-drying could be significantly reduced in freeze-drying. This conclusion was further evidenced by the 8 times higher BET surface

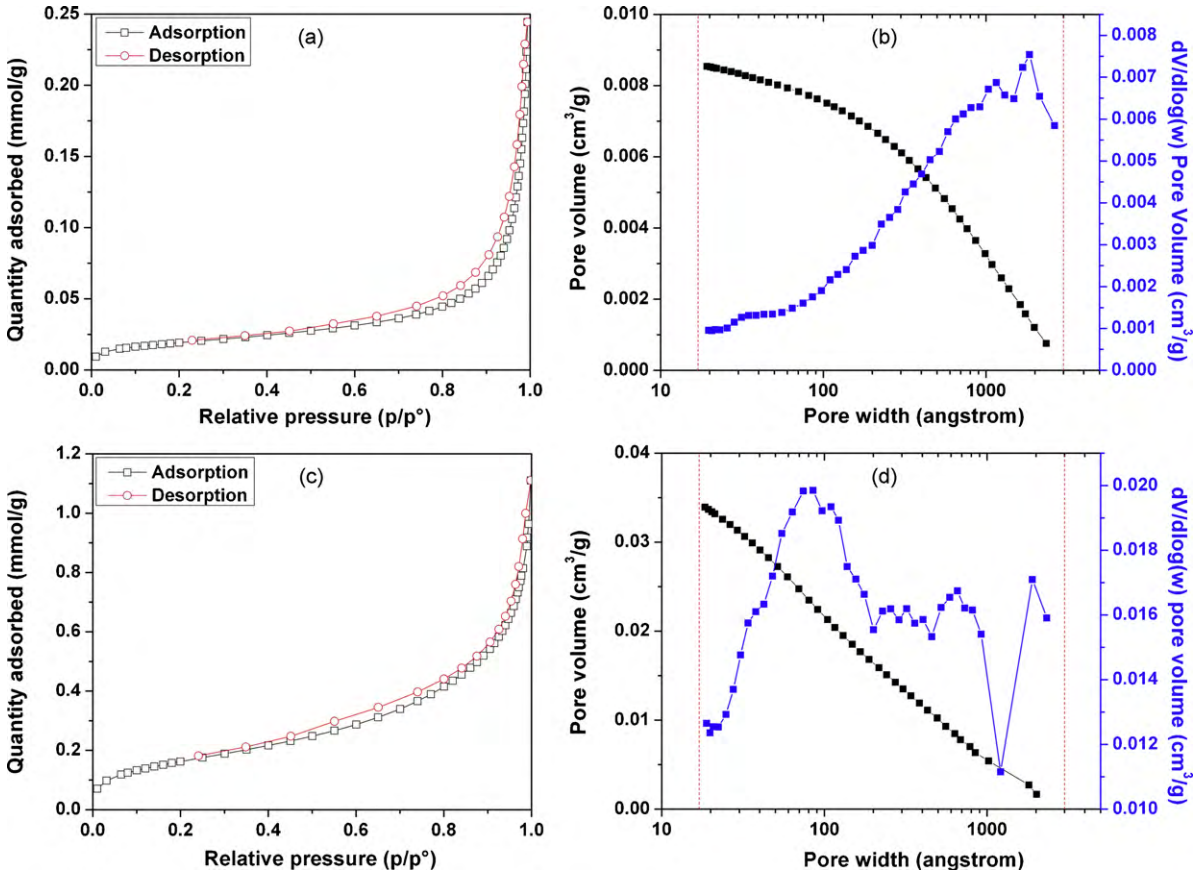

Fig. 7. N_2 adsorption and desorption isotherms at 77 K of cellulose (a) powder and (c) nanocrystals. BJH pore size distribution derived from adsorption isotherm of cellulose (b) powder and (d) nanocrystals.

Table 1
BET surface areas and pore characteristics of cellulose powder and nanocrystals.

	BET surface area (m^2/g)	*t*-Plot external surface area (m^2/g)	BJH adsorption cumulative surface area of pores (m^2/g)[a]	BJH adsorption cumulative volume of pores (cm^3/g)[a]	BJH adsorption average pore width (4V/A) (Å)
Cellulose powders	1.547 ± 0.012	1.480 ± 0.032	1.563 ± 0.019	0.00839 ± 0.00026	214.64 ± 7.23
Cellulose nanocrystals	13.362 ± 0.034	15.093 ± 0.215	14.771 ± 0.158	0.03396 ± 0.00059	91.99 ± 2.57

[a] Between 17 and 3000 Å.

area of cellulose nanocrystals (13.362 m^2/g) compared to that of the original cellulose (1.547 m^2/g).

4. Conclusions

Cellulose nanocrystals with rod, sphere, and network-structured morphologies were prepared by acid hydrolysis and freeze-drying of cotton cellulose. Hydrolysis with sulfuric acid removed amorphous cellulose to produce isolated cellulose nanocrystals with newly introduced sulfate groups on the nanocrystal surfaces. Repulsion among the negatively charged cellulose nanocrystals and quick freezing with liquid nitrogen were very effective in preventing aggregate formation driven by the strong hydrogen bonding. The cellulose nanocrystals retained their chemical and Iβ crystalline structures, while exhibited significantly different thermal and decomposition behaviors, suggesting higher thermal conductivity and possibly direct solid-to-gas decomposition mechanism. These cellulose nanocrystals could be readily and directly dispersed into water, ethanol, DMF and other solvents without any additional preparation or aids. Furthermore, the cellulose nanocrystals formed a mesoporous structure with a mean pore width of 91.99 ± 2.57 Å and possessed a high surface area of 13.362 m^2/g. The results demonstrated that the acid hydrolysis not only produced nanocrystalline structures but also introduced surface charges for their effective separation. Coupling with freeze-drying, the cellulose nanocrystals exhibit the desirable quick re-dispersion capability which is essential for their practical applications.

Acknowledgement

This research was made possible by funding from the National Textile Center (project M02-CD05), the Jastro-Shields Graduate Research Award, and Summer Graduate Researcher Award from the University of California, Davis.

References

Beck-Candanedo, S., Roman, M., & Gray, D. G. (2005). Effect of reaction conditions on the properties and behavior of wood cellulose nanocrystal suspensions. *Biomacromolecules*, *6*(2), 1048–1054.

Beecher, J. F. (2007). Organic materials: Wood, trees and nanotechnology. *Nature Nanotechnology*, *2*(8), 466–467.

Dong, S., & Roman, M. (2007). Fluorescently labeled cellulose nanocrystals for bioimaging applications. *Journal of the American Chemical Society*, *129*(45), 13810–13811.

Favier, V., Chanzy, H., & Cavaille, J. Y. (1995). Polymer nanocomposites reinforced by cellulose whiskers. *Macromolecules*, *28*(18), 6365–6367.
Grunert, M., & Winter, W. T. (2002). Nanocomposites of cellulose acetate butyrate reinforced with cellulose nanocrystals. *Journal of Polymers and the Environment*, *10*(1/2), 27–30.
Hanley, S. J., Giasson, J., Revol, J. F., & Gray, D. G. (1992). Atomic force microscopy of cellulose microfibrils: Comparison with transmission electron microscopy. *Polymer*, *33*(21), 4639–4642.
Helbert, W., Cavaille, J. Y., & Dufresne, A. (1996). Thermoplastic nanocomposites filled with wheat straw cellulose whiskers. Part I: Processing and mechanical behavior. *Polymer Composites*, *17*(4), 604–611.
Helbert, W., Chanzy, H., Husum, T. L., Schuelein, M., & Ernst, S. (2003). Fluorescent cellulose microfibrils as substrate for the detection of cellulase activity. *Biomacromolecules*, *4*(3), 481–487.
Hon, D. N. S., & Shiraishi, N. (1991). *Wood and cellulosic chemistry*. New York: M. Dekker.
Ifuku, S., Nogi, M., Abe, K., Handa, K., Nakatsubo, F., & Yano, H. (2007). Surface modification of bacterial cellulose nanofibers for property enhancement of optically transparent composites: Dependence on acetyl-group DS. *Biomacromolecules*, *8*(6), 1973–1978.
Kim, J., Yun, S., & Ounaies, Z. (2006). Discovery of cellulose as a smart material. *Macromolecules*, *39*(12), 4202–4206.
Lu, P., & Hsieh, Y.-L. (2009). Cellulose nanocrystal-filled poly(acrylic acid) nanocomposite fibrous membranes. *Nanotechnology*, *20*(41), 415604/415601–415604/415609.
Marchessault, R. H., Morehead, F. F., & Koch, M. J. (1961). Hydrodynamic properties of neutral suspensions of cellulose crystallites as related to size and shape. *Journal of Colloid Science*, *16*, 327–344.
Mo, Z.-l., Zhao, Z.-l., Chen, H., Niu, G.-p., & Shi, H.-f. (2009). Heterogeneous preparation of cellulose-polyaniline conductive composites with cellulose activated by acids and its electrical properties. *Carbohydrate Polymers*, *75*(4), 660–664.
Podsiadlo, P., Choi, S.-Y., Shim, B., Lee, J., Cuddihy, M., & Kotov, N. A. (2005). Molecularly engineered nanocomposites: Layer-by-layer assembly of cellulose nanocrystals. *Biomacromolecules*, *6*(6), 2914–2918.
Podsiadlo, P., Sui, L., Elkasabi, Y., Burgardt, P., Lee, J., Miryala, A., et al. (2007). Layer-by-layer assembled films of cellulose nanowires with antireflective properties. *Langmuir*, *23*(15), 7901–7906.
Roman, M., & Winter, W. T. (2004). Effect of sulfate groups from sulfuric acid hydrolysis on the thermal degradation behavior of bacterial cellulose. *Biomacromolecules*, *5*(5), 1671–1677.
Sakurada, I., Nukushina, Y., & Ito, T. (1962). Experimental determination of the elastic modulus of crystalline regions in oriented polymers. *Journal of Polymer Science*, *57*, 651–660.
Samir, M. A. S. A., Alloin, F., & Dufresne, A. (2005). Review of recent research into cellulosic whiskers. Their properties and their application in nanocomposite field. *Biomacromolecules*, *6*(2), 612–626.
Saxena, I. M., & Brown, R. M., Jr. (2005). Cellulose biosynthesis: Current views and evolving concepts. *Annals of Botany (Oxford, United Kingdom)*, *96*(1), 9–21.
Shimazaki, Y., Miyazaki, Y., Takezawa, Y., Nogi, M., Abe, K., Ifuku, S., et al. (2007). Excellent thermal conductivity of transparent cellulose nanofiber/epoxy resin nanocomposites. *Biomacromolecules*, *8*(9), 2976–2978.
Sing, K. S. W., Everett, D. H., Haul, R. A. W., Moscou, L., Pierotti, R. A., Rouquerol, J., et al. (1985). Reporting physisorption data for gas/solid systems with special reference to the determination of surface area and porosity (Recommendations 1984). *Pure and Applied Chemistry*, *57*(4), 603–619.
Sturcova, A., Davies, G. R., & Eichhorn, S. J. (2005). Elastic modulus and stress-transfer properties of tunicate cellulose whiskers. *Biomacromolecules*, *6*(2), 1055–1061.
Svagan, A. J., Samir, M. A. S. A., & Berglund, L. A. (2008). Biomimetic foams of high mechanical performance based on nanostructured cell walls reinforced by native cellulose nanofibrils. *Advanced Materials*, *20*(7), 1263.
Terech, P., Chazeau, L., & Cavaille, J. Y. (1999). A small-angle scattering study of cellulose whiskers in aqueous suspensions. *Macromolecules*, *32*(6), 1872–1875.
Tingaut, P., Zimmermann, T., & Lopez-Suevos, F. (2010). Synthesis and characterization of bionanocomposites with tunable properties from poly(lactic acid) and acetylated microfibrillated cellulose. *Biomacromolecules*, *11*(2), 454–464.
van den Berg, O., Capadona, J. R., & Weder, C. (2007). Preparation of homogeneous dispersions of tunicate cellulose whiskers in organic solvents. *Biomacromolecules*, *8*(4), 1353–1357.
Wada, M., Heux, L., & Sugiyama, J. (2004). Polymorphism of cellulose I family: Reinvestigation of cellulose IVI. *Biomacromolecules*, *5*(4), 1385–1391.
Wada, M., Kondo, T., & Okano, T. (2003). Thermally induced crystal transformation from cellulose I.alpha. to I.beta. *Polymer Journal (Tokyo Japan)*, *35*(2), 155–159.
Wong, E. W., Sheehan, P. E., & Lieber, C. M. (1997). Nanobeam mechanics: Elasticity, strength, and toughness of nanorods and nanotubes. *Science (Washington, DC)*, *277*(5334), 1971–1975.
Yu, M.-F., Lourie, O., Dyer, M. J., Moloni, K., Kelly, T. F., & Ruoff, R. S. (2000). Strength and breaking mechanism of multiwalled carbon nanotubes under tensile load. *Science*, *287*(5453), 637–640.
Zhang, J. G., Elder, T. J., Pu, Y. Q., & Ragauskas, A. J. (2007). Facile synthesis of spherical cellulose nanoparticles. *Carbohydrate Polymers*, *69*(3), 607–611.
Zuluaga, R., Putaux, J. L., Cruz, J., Velez, J., Mondragon, I., & Ganan, P. (2009). Cellulose microfibrils from banana rachis: Effect of alkaline treatments on structural and morphological features. *Carbohydrate Polymers*, *76*(1), 51–59.